The mobility of dual vortices in honeycomb, square, triangular, Kagome and dice lattices

2006 J. Phys.: Condens. Matter 18 6907

(http://iopscience.iop.org/0953-8984/18/29/028)

INSTITUTE OF PHYSICS PUBLISHING JOURNAL OF PHYSICS: CONDENSED MATTER

J. Phys.: Condens. Matter **18** (2006) 6907–6922 doi:10.1088/0953-8984/18/29/028

The mobility of dual vortices in honeycomb, square, triangular, Kagome and dice lattices

Longhua Jiang and Jinwu Ye

Physics Department, The Pennsylvania State University, University Park, PA 16802, USA

Received 4 May 2006
Published 6 July 2006
Online at stacks.iop.org/JPhysCM/18/6907

Abstract

It was known that by a duality transformation, interacting bosons at filling factor $f = p/q$ hopping on a lattice can be mapped to interacting vortices hopping on the dual lattice subject to a fluctuating *dual* 'magnetic field' whose average strength through a dual plaquette is equal to the boson density $f = p/q$. So the kinetic term of the vortices is the same as the Hofstadter problem of electrons moving in a lattice in the presence of $f = p/q$ flux per plaquette. Motivated by this mapping, we study the Hofstadter bands of vortices hopping in the presence of magnetic flux $f = p/q$ per plaquette on five most common bipartite and frustrated lattices namely square, honeycomb, triangular, dice and Kagome lattices. We count the total number of bands, and determine the number of minima and their locations in the lowest band. We also numerically calculate the bandwidths of the lowest Hofstadter bands in these lattices that directly measure the mobility of the dual vortices. The less mobile the dual vortices are, the more likely are the bosons to be in a superfluid state. We find that apart from the Kagome lattice at odd q, they all satisfy the exponential decay law $W = Ae^{-cq}$ even at the smallest q. At given q, the bandwidth W decreases in the order of triangle, square and honeycomb lattice. This indicates that the domain of the superfluid state of the original bosons increases in the order of the corresponding direct lattices: honeycomb, square and triangular. When $q = 2$, we find that the lowest Hofstadter band is completely flat for both Kagome and dice lattices. There is a gap on the Kagome lattice, but no gap on the dice lattice. This indicates that the boson ground state at half filling with nearest neighbour hopping on Kagome lattice is always a superfluid state. The superfluid state remains stable slightly away from the half filling. Our results show that the behaviours of bosons at or near half filling on Kagome lattices are quite distinct from those in square, honeycomb and triangular lattices studied previously.

(Some figures in this article are in colour only in the electronic version)

1. Introduction

The extended boson Hubbard model with various kinds of interactions, for various kinds of lattice (bipartite or frustrated) with various kinds of filling factor (commensurate $f = p/q$ or incommensurate) is described by the following Hamiltonian [5–7]:

$$H = -t\sum_{\langle ij\rangle}(b_i^\dagger b_j + \text{h.c.}) - \mu\sum_i n_i + \frac{U}{2}\sum_i n_i(n_i-1) + V_1\sum_{\langle ij\rangle} n_i n_j + V_2\sum_{\langle\langle ik\rangle\rangle} n_i n_k + \cdots \tag{1}$$

where $n_i = b_i^\dagger b_i$ is the boson density and U, V_1, V_2 are onsite, nearest neighbour (nn) and next nearest neighbour (nnn) interactions between the bosons. The $\cdots$ may include further neighbour interactions and possible ring-exchange interactions. For a bipartite lattice, the sign of t can be changed by changing the sign of b_i in one of the two sublattices. But in a frustrated lattice, the sign of t makes a difference.

It is very important to extend boson Hubbard model in bipartite lattices to frustrated lattices such as triangular, dice and Kagome lattices, because of the following motivations.

(1) For atatoms adsorptions on bare graphite, the preferred adsorption sites form a triangular lattice. The phase diagrams of coverage (the filling factor) versus temperature resulting from the competitions of these energy scales are very diverse and rich [1, 2]. It was believed that equation (1) may capture the main physics of the phenomena.

(2) Atomic physicists are trying to construct effective two-dimensional frustrated optical lattices using laser beams and then loading either ultra-cold fermion or boson atoms at different filling factors on the lattice. They may tune the parameters to realize different phases by going through quantum phase transitions [3, 4].

(3) In the hard-core limit $U \to \infty$, due to the exact mapping between the boson operator and the spin $s = 1/2$ operator, $b_i^\dagger = S_i^+, b_i = S_i^-, n_i = S_i^z + 1/2$, the boson model equation (1) can be mapped to an anisotropic $S = 1/2$ quantum spin model in an external magnetic field [7, 6]:

$$H = -2t\sum_{\langle ij\rangle}(S_i^x S_j^x + S_i^y S_j^y) + V_1\sum_{\langle ij\rangle} S_i^z S_j^z + V_2\sum_{\langle\langle ik\rangle\rangle} S_i^z S_k^z - h\sum_i S_i^z + \cdots \tag{2}$$

where $h = \mu - 2V_1 - 2V_2$ for a square lattice. Note that in this Hamiltonian, there is a ferromagnetic coupling in the XY spin components and antiferromagnetic coupling in the Z spin component. Again, in a bipartite lattice, the sign of t can be changed by changing the sign of S_i^x, S_i^y in one of the two sublattices, but keeping S_i^z untouched, so equation (2) is the same as that for a quantum Heisenberg antiferromagnet (QHA). However, in a frustrated lattice, the sign of t makes a difference, so equation (2) is quite different from that for the QHA. The one to one correspondence between physical quantities in the boson model and those in the spin model means that the boson density corresponds to the magnetization $n \leftrightarrow M$, the chemical potential corresponds to the magnetic field $\mu \leftrightarrow h$, and the compressibility corresponds to the susceptibility $\kappa = \frac{\partial n}{\partial \mu} \leftrightarrow \chi = \frac{\partial M}{\partial h}$. The boson number conservation corresponds to the $U(1)$ rotation around the $\hat{z}$ axis, the superfluid state $\langle b_i\rangle \neq 0$ corresponds to the XY ordered state $\langle S_i^+\rangle \neq 0$, and the charge ordered state corresponds to the modulation of $\langle S^z\rangle$. The supersolid corresponds to the simultaneous $\langle S_i^+\rangle \neq 0$ and the modulation of $\langle S_i^z\rangle$ [6, 7]. In the hard-core limit, equation (1) at half filling ($q = 2$) has the particle–hole (P–H) symmetry $b_i \leftrightarrow b_i^\dagger, n_i \to 1 - n_i$; it can be mapped to equation (2) in zero magnetic field $h = 0$ with the time-reversal symmetry

$S_i^+ \to -S_i^-, S_i^z \to -S_i^z$. Equation (1) on triangular lattice at $q = 2$ is the prototype model for studying the supersolid state with P–H symmetry [7].

The model equation (1) with only the onsite interaction on a square lattice was first studied in [5]. The effects of long-range Coulomb interactions on the transition were studied in [8]. Very recently, the most general cases in a square lattice at generic commensurate filling factors $f = p/q$ (p, q are relative prime numbers) were systematically studied in [9]. After performing the charge–vortex duality transformation [13], the authors in [9] obtained a dual theory of equation (1) in terms of the interacting vortices ψ_a hopping on the dual lattice subject to a fluctuating *dual* 'magnetic field'. The average strength of the dual 'magnetic field' through a dual plaquette is equal to the boson density $f = p/q$. This is similar to the Hofstadter problem of electrons moving in a crystal lattice in the presence of a magnetic field [10]. The magnetic space group (MSG) in the presence of this dual magnetic field dictates that there are at least q-fold degenerate minima in the mean field energy spectrum. The q minima can be labelled as $\psi_l, l = 0, 1, \ldots, q-1$, which forms a q-dimensional representation of the MSG. In the continuum limit, the final effective theory describing the superconductor to the insulator transition in terms of these q order parameters should be invariant under this MSG. If $\langle\psi_l\rangle = 0$ for every $l = \pm$, the system is in the superfluid state. If $\langle\psi_l\rangle \neq 0$ for at least one l, the system is in the insulating state. In the *supersolid* state [6, 7, 12], one condenses a *vortex–antivortex pair*, but still keeps $\langle\psi_l\rangle = 0$ for every l. In the insulating or supersolid state, there must exist some kind of charge density wave (CDW) (we assume that every boson carries one internal charge) or valence bond solid (VBS) states which may be stabilized by longer range interactions or possible ring exchange interactions included in equation (1). Very recently, the dual method was used to study the extended Boson Hubbard model on a triangular lattice [11].

In a recent paper [12], one of the authors applied the dual approach of the extended boson Hubbard model equation (1) to study the reentrant 'superfluid' in a narrow region of coverages in the second layer of ^{4}He adsorbed on graphite detected by Crowell and Reppy's torsional oscillator experiment in 1993 [15, 16]. He showed that there are two consecutive transitions at zero temperature *driven by the coverage*: a commensurate-charge density wave (CDW) at half filling to a narrow window of supersolid, then to an incommensurate-CDW. In the Ising limit, the supersolid is a CDW supersolid, whereas in the easy-plane limit, it is a valence bond supersolid. Both transitions are second-order transitions with exact critical exponents $z = 2, \nu = 1/2, \eta = 0$. The results concluded that ^{4}He lattice supersolid was already observed in 1993. He also applied the same dual method to study the H_2/Kr/graphite system investigated in a recent experiment [14] and proposed that a judicious choice of substrate could also lead to an occurrence of hydrogen lattice supersolid. Implications of the realizations of a lattice supersolid of ultra-cold atoms in optical lattices were also given in [12].

Note that in the dual vortex picture, there are always interactions between vortices. Because the phase factors from the dual magnetic field only appear in the kinetic term, the interactions always commute with any generators in the MSG, so they will not change the symmetry of the MSG.

In this paper, we study the Hofstadter bands of vortices hopping in the presence of a dual magnetic field $f = p/q$ on the five most common bipartite and frustrated lattices namely square, honeycomb, triangular, dice and Kagome lattices. We especially study the bandwidth of the lowest bands. There are at least two motivations to study the bandwidth of the lowest bands. (1) As pointed out in [9], as q becomes too large, the dual vortex method suffers the following two drawbacks. (a) As dictated by the MSG, there are q minima in the Brillouin zone (BZ), so the distance in momentum space between these minima scales as $1/q$; the continuum theory only works at $k \ll 1/q$, and therefore applies only at distance $\gg q$. The validity

regime of the dual vortex theory shrinks. (b) When integrating out the vortex modes away from the minima, one encounters energy denominators determined by this bandwidth, so the dual vortex method may completely break down if the bandwidth becomes too small. By a simple argument, they estimated that at large q, the bandwidth W of the lowest Hofstadter band scales as $W \sim e^{-cq}$ with c at the order of 1.[1] So the smaller the bandwidth, the smaller the valid regime of the dual vortex approach. (2) In the dual vortex picture, there are both a kinetic energy term and interactions between vortices. The kinetic term favours the moving of the vortices, while the interactions favour the localization of the vortices; the competition of the two energy scales may result in all kinds of phases such as superfluid, CDW, VBS and even supersolid phase [12]. In this paper, we focus on the kinetic term only. Calculating the bandwidth of the kinetic term is very important, because the smaller of the bandwidth, the more inert the vortices (the less mobile the vortices are); therefore the boson superfluid state is more likely to occur.

By choosing suitable gauges and solving the corresponding Harper equations in the five lattices, we count the number of bands, and determine the number of minima and their locations in the lowest Hofstadter bands. The results are listed in table 1. We also numerically calculate the bandwidths of the lowest bands in these lattices at any q and test against the estimate $W \sim Ae^{-cq}$. We believe that although the argument in [9] seems reasonable, it is far from being convincing. So it is important to test this argument by quantitative numerical calculations. We find that apart from the Kagome lattice at odd q, the exponential law is indeed satisfied, and determine (A, c) for the five different lattices. The results are listed in table 2. We find that at given q, the bandwidth W decreases in the order of triangle, square and honeycomb lattice. The corresponding direct lattices are honeycomb, square and triangular lattices, so the tendency to form a superfluid state increases. As shown in table 2, when $q = 2$, the lowest bands in both dice and Kagome lattices are flat. In the dice lattice, the gap between the second flat band and the lowest flat band is $\sqrt{6}$. This indicates that for the original boson at half filling with nearest neighbour hopping on the Kagome lattice, there could be only a superfluid state. However, in the Kagome lattice, the gap between the second dispersive band and the lowest flat band vanishes at $\vec{k} = (0, 0)$, so the second dispersive band cannot be ignored even in the lowest energy limit. Due to the gap vanishing on the Kagome lattice, we cannot say definite things about the ground state in the original boson on a dice lattice. There are some previous results on the energy spectra on square, honeycomb and triangular lattices [9, 12, 11, 17, 19] with different focuses. Our results on dual dice and Kagome lattices, especially the discussions on the possible boson ground states on corresponding direct lattices, are new and most interesting.

There are two equivalent methods to be used to study the Hofstadter bands. One is the magnetic Brillouin zone (MBZ) method to be employed in the main text. This method is physically more transparent and intuitive. Another is the symmetric method used in [9] and to be used in the appendix. This method treats the x and y coordinates on an equal footing, so is more symmetric than the first one. In the main text, we will use the first method to derive the Harper equations in the five lattices and then solve the equations analytically at small q and numerically at large q. In the appendix, we will use the second method to repeat the calculations. Although the coefficients of the Harper equations in the two schemes are different, as expected, we find that they result in the same energy spectra.

In the following, we will first study two bipartite lattices, namely square and honeycomb lattices, then we will investigate three frustrated lattices namely triangular, dice and Kagome lattices. In the final section, we summarize our results in tables 1 and 2, and we also comment

[1] This bandwidth is much smaller than the Landau level cyclotron gap $\sim 1/q$ in the limit of large q. In this limit, the magnetic flux through one plaquette gets very small, so one is approaching the continuum limit where the Landau levels have zero width.

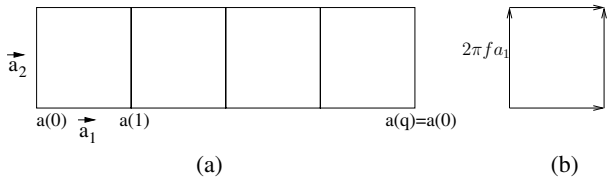

Figure 1. (a) A magnetic unit cell of a square lattice, (b) phase factors on bonds; 0 phase factors are not shown.

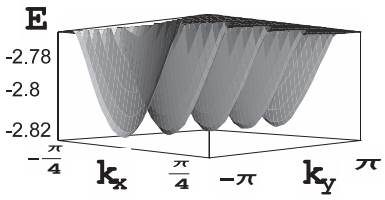

Figure 2. The lowest energy band of a square lattice at $q = 4$.

on the results on CDW formations in high temperature superconductors claimed in [9] where q values as large as 8, 16, 32 are used. In most of the cases, we focus on the $p = 1$ case.

2. Square lattice

We are looking at the Hofstadter band of vortices hopping around a square lattice in the presence of magnetic flux $f = p/q$ per square [9] (figure 1). In the MBZ method, one magnetic unit cell is q times larger than the conventional unit cell (figure 1(a)). For the simplest gauge chosen in figure 1(b), the hopping Hamiltonian is

$$H = -t \sum_{\vec{x}} [|\vec{x} + \vec{a}_1\rangle\langle\vec{x}| + |\vec{x} + \vec{a}_2\rangle e^{i2\pi f a_1}\langle\vec{x}| + \text{h.c.}]. \tag{3}$$

In the following, for simplicity, we set $t = 1$. The eigenvalue equation $H\psi(\vec{k}) = E(\vec{k})\psi(\vec{k})$ leads to the Harper equation:

$$-e^{-ik_x}\psi_{l-1}(\vec{k}) - 2\cos(2\pi f l + k_y)\psi_l(\vec{k}) - e^{ik_x}\psi_{l+1}(\vec{k}) = E(\vec{k})\psi_l(\vec{k}) \tag{4}$$

where $l = 0, \ldots, q-1$; $\frac{-\pi}{q} \leqslant k_x \leqslant \frac{\pi}{q}$; $-\pi \leqslant k_y \leqslant \pi$.

For small values of q, equation (4) can be solved analytically. For large values of q, we solve it numerically. There are always q bands. We focus on the lowest energy band and its bandwidth. As shown in [9], there are q minima at $(0, 2\pi f l)$, $l = 0, \ldots, q-1$. The spectrum for $q = 4$ is shown in figure 2. In order to see clearly all the four MSG-related minima, only part of the energy band close to the four minima in the lowest band is included. We also numerically calculated the bandwidth of the lowest band up to $q = 18$. We found that it indeed satisfies the exponential law $W = Ae^{-cq}$ with $A = 26.05$, $c = -1.20$. In a semi-log plot, this is a straight line, which is shown in figure 3.

What is surprising is that even for the smallest $q = 1$, which is the no magnetic field case, the exponential law is still satisfied.

3. Honeycomb lattice

The honeycomb lattice is not a Bravais lattice: it can be thought of as an underlying parallelogram Bravais lattice with two primitive vectors $\vec{a}_1 = \hat{x}$, $\vec{a}_2 = \frac{1}{2}\hat{x} + \frac{\sqrt{3}}{2}\hat{y}$ plus a two-

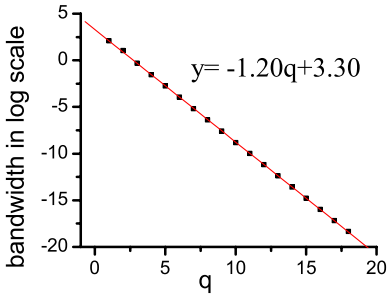

Figure 3. The bandwidth of the lowest band in a square lattice versus q.

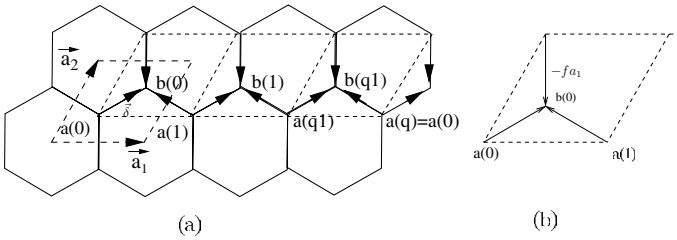

Figure 4. (a) A magnetic unit cell of a honeycomb lattice, (b) phase factors on bonds; 0 phase factors are not shown.

point basis located at $\vec{x}+\vec{\delta}$ and $\vec{x}+2\vec{\delta}$ where $\vec{\delta}=\frac{1}{3}(\vec{a}_1+\vec{a}_2)$ (figure 2). Its reciprocal lattice is also a parallelogram Bravais lattice spanned by $\vec{k}=k_1\vec{b}_1+k_2\vec{b}_2$ with $\vec{b}_i\cdot\vec{a}_j=\delta_{ij}$.

In the MBZ method, one magnetic unit cell is q times larger than the conventional unit cell (figure 4(a)). In one conventional unit cell, there are also two atoms which are labelled by two colour indices a and b (figure 4). We are looking at the Hofstadter band of vortices hopping around a honeycomb lattice in the presence of magnetic flux $f=p/q$ per hexagon. For the simplest gauge chosen in figure 4(b), the vortex hopping Hamiltonian is

$$H=-t\sum_{\vec{x}}[|\vec{x}+\vec{\delta}\rangle\langle\vec{x}|+|\vec{x}+\vec{\delta}\rangle\langle x+\vec{a}_1|+|\vec{x}+\vec{\delta}\rangle e^{-i2\pi f a_1}\langle\vec{x}+\vec{a}_2|+\text{h.c.}]. \tag{5}$$

The Harper equation is

$$\begin{aligned}-(1+e^{i(k_x+2\pi fl)})\psi_l^a(\vec{k})-e^{ik_y}\psi_{l+1}^a(\vec{k})&=E(\vec{k})\psi_l^b(\vec{k})\\ -(1+e^{-i(k_x+2\pi fl)})\psi_l^b(\vec{k})-e^{-ik_y}\psi_{l-1}^b(\vec{k})&=E(\vec{k})\psi_l^a(\vec{k})\end{aligned} \tag{6}$$

where $l=0,\ldots,q-1$ are the flavour indices and a,b are the colour indices, $-\frac{\pi}{q}\leqslant k_x\leqslant\frac{\pi}{q}$.

For small values of q, equation (6) can be solved analytically. When $q=1$, there is actually no magnetic field; this is just the ordinary tight-binding model. There are two bands: $\pm\sqrt{3+2(\cos k_x+\cos k_y+\cos(k_x+k_y))}$. The lowest energy band is $-\sqrt{3+2(\cos k_x+\cos k_y+\cos(k_x+k_y))}$. There is only one minimum at $(0,0)$. The bandwidth is 3. The $q=2$ case is especially interesting, because the original boson model can be mapped to a quantum $s=1/2$ spin model equation (2) in a triangular lattice at zero field. For $q=2$, there are four bands $E(\vec{k})=\pm t\sqrt{3\pm\sqrt{2A(\vec{k})}}$ where $A(\vec{k})=3+(\cos 2k_1+\cos 2k_2-\cos(2k_1-2k_2))$. The lowest subband is $E(\vec{k})=-t\sqrt{3+\sqrt{2A(\vec{k})}}$. There are four minima at $\pm(\pi/6,-\pi/6)$ and $\pm(\pi/6,5\pi/6)$. The four minima transform to each other under the MSG.

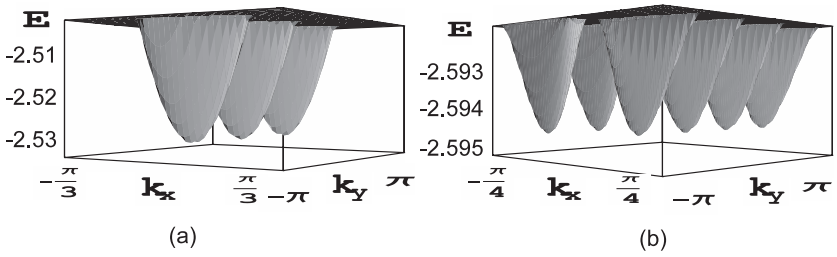

Figure 5. The lowest energy bands of a honeycomb lattice at (a) $q = 3$, (b) $q = 4$.

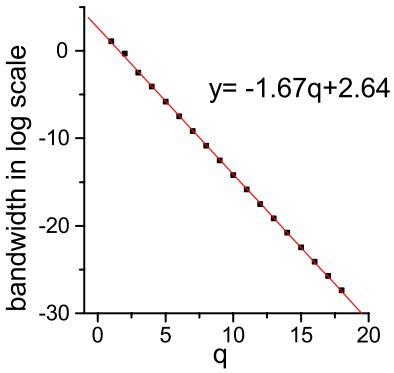

Figure 6. The bandwidth of a honeycomb lattice versus q.

For general q, there are always $2q$ bands. As shown in [11, 17], there are two cases. (1) q is odd: there are q minima at $(0, 2\pi fl), l = 0, \ldots, q-1$. (2) q is even: there are $2q$ minima at $(\frac{\alpha\pi}{3q}, -\frac{\alpha\pi}{3q} + 2\pi fl)$ where $\alpha = \pm, l = 0, \ldots, q-1$.

For large values of q, we solve equation (6) numerically. Just like in square lattice, we focus on the energy band near the minima in the lowest energy band. The $q = 3$ and $q = 4$ spectra are shown in figures 5(a) and (b) respectively.

We also numerically calculated the bandwidths of the lowest band up to $q = 18$. We found that they satisfy the exponential law $W = Ae^{-cq}$ with $A = 11.82, c = -1.66$ for both q even and odd. In a semi-log plot, this is a straight line, which is shown in figure 6.

What is surprising is that even for the smallest $q = 1$, which is the no magnetic field case, the exponential law is still satisfied.

4. Triangular lattice

In the previous two sections, we studied two bipartite lattices. In this section, we study the simplest frustrated lattice, which is the triangular lattice. As was said in the introduction, the physics in frustrated lattices could be very different from that in bipartite lattices.

We are looking at the Hofstadter band of vortices hopping around a triangular lattice in the presence of magnetic flux $f = p/q$ per triangle. For the simplest gauge chosen in figure 7(b), the Hamiltonian is

$$H = -t \sum_{\vec{x}} [|\vec{x} + \vec{a}_1\rangle\langle\vec{x}| + |\vec{x} + \vec{a}_2\rangle e^{i2\pi 2fa_1}\langle\vec{x}| + |\vec{x} + \vec{a}_1 + \vec{a}_2\rangle e^{i2\pi 2f(a_1+\frac{1}{2})}\langle\vec{x}| + \text{h.c.}]. \quad (7)$$

The corresponding Harper equation is

$$\begin{aligned} &-2\cos(k_y + 2\pi fl)\psi_l(\vec{k}) - (e^{-ik_x} + e^{-i(k_x+k_y+2\pi f(2l-1))})\psi_{l-1}(\vec{k}) \\ &\quad -(e^{ik_x} + e^{i(k_x+k_y+2\pi f(2l+1))})\psi_{l+1}(\vec{k}) = E(\vec{k})\psi_l(\vec{k}) \end{aligned} \quad (8)$$

where $l = 0, \ldots, q-1$.

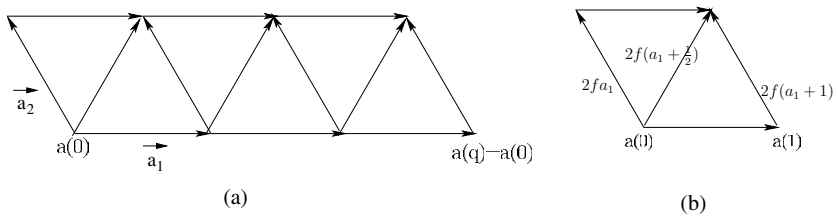

Figure 7. Triangular lattice: (a) magnetic unit cell of a triangular lattice, (b) phase factors on bonds; 0 phase factors are not shown.

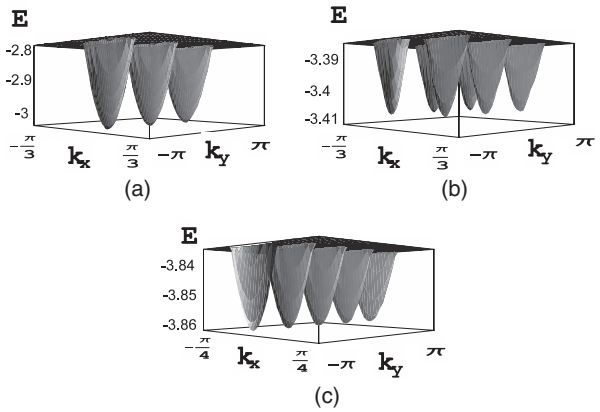

Figure 8. The lowest energy bands of a triangular lattice at (a) $q = 3$, (b) $q = 6$, and (c) $q = 8$.

From the phase factors on the bond, it is easy to see that when q is even, there are only $\frac{q}{2}$ unit cells in one magnetic unit cell. Since the magnetic unit cell shrinks to $\frac{q}{2}$, the range of k_x in the momentum space doubles its range accordingly. Therefore in equation (8), for q odd, $-\frac{\pi}{q} \leqslant k_x \leqslant \frac{\pi}{q}$, while for q even, $-\frac{2\pi}{q} \leqslant k_x \leqslant \frac{2\pi}{q}$.

In fact, as shown in [9], there are three cases in a triangular lattice. (1) When q is odd, there are q bands. There are q minima at $(0, 4\pi fl)$, $l = 0, \ldots, q-1$ in the lowest band. (2) When q is even, there are $q/2$ bands. There are still two subcases. (2a) When $q = 2n$ with n odd, there are q minima at $(\frac{2\pi\alpha}{3q}, \frac{2\pi\alpha}{3q} + 4\pi fl)$, $\alpha = \pm$ and $l = 0, \ldots, \frac{q}{2} - 1$. (2b) When $q = 2n$ with n even, there are $\frac{q}{2}$ minima at $(0, 4\pi fl)$, $l = 0, \ldots, \frac{q}{2} - 1$.

For $q = 1$, which is the no magnetic field case, the energy spectrum is $E(\vec{k}) = -2(\cos k_x + \cos k_y + \cos(k_x + k_y))$; there is only one minimum at $(0, 0)$. For $q = 2$, as shown in [12], the spectrum is $E(\vec{k}) = -2(\cos k_x + \cos k_y - \cos(k_x + k_y))$. There are two minima located at $(\pm\frac{\pi}{3}, \pm\frac{\pi}{3})$

For large q, we solve equation (8) numerically. The results for $q = 3$ (odd case), $q = 6$ ($2n$ with n odd case) and $q = 8$ ($2n$ with n even case) are shown in figures 8(a)–(c) respectively.

We also numerically calculated the bandwidth of the lowest band up to $q = 25$ for q odd and up to $q = 30$ for q even. For q odd, we find $A = 9.21, c = 0.82$ (figure 9(a)). For $q = 2n$, n both odd and even, the bandwidth satisfies the same exponential law with $A = 55.70, c = 0.83$ (figure 9(b)).

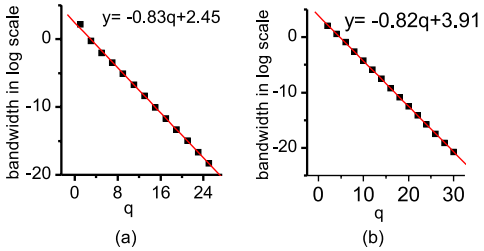

Figure 9. The bandwidth of a triangular lattice versus q: (a) q is odd,(b) q is even.

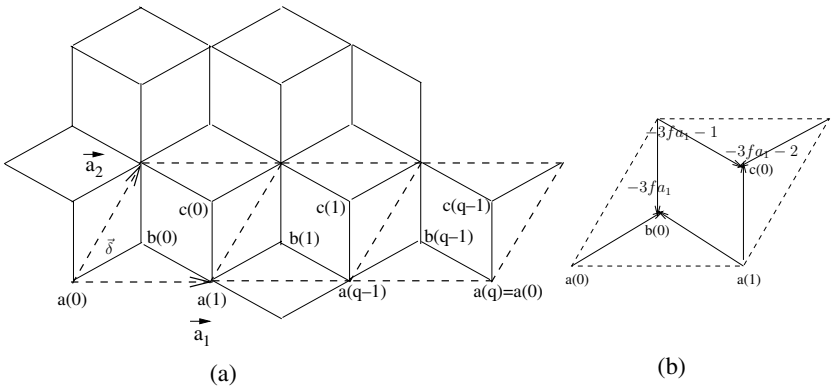

Figure 10. Dice lattice: (a) magnetic unit cell of a dice lattice, (b) phase factors on bonds; 0 phase factors are not shown.

5. Dice lattice

The dice lattice is the dual lattice of the Kagome lattice. It can be thought of as consisting of two interpenetrating honeycomb lattices. Obviously, the dice lattice is not a Bravais lattice; it can be thought of as an underlying parallelogram Bravais lattice with two primitive lattice vectors $\vec{a}_1 = \hat{x}, \vec{a}_2 = \frac{1}{2}\hat{x} + \frac{\sqrt{3}}{2}\hat{y}$ plus a three-point basis labelled a, b, c located at $\vec{x}, \vec{x} + \vec{\delta}, \vec{x} + 2\vec{\delta}$ where $\vec{\delta} = \frac{1}{3}(\vec{a}_1 + \vec{a}_2)$ (figure 10). In contrast to the honeycomb lattice shown in figure 4, the dice lattice is not a bipartite lattice and has a three-sublattice structure.

We are looking at the Hofstadter band of vortices hopping around a dice lattice in the presence of magnetic flux $f = p/q$ per parallelogram. For the simplest gauge chosen in figure 10(b), the Hamiltonian is

$$\begin{aligned} H = -t \sum_{\vec{x}} [&|\vec{x} + \vec{\delta}\rangle\langle\vec{x}| + |\vec{x} + \vec{\delta}\rangle e^{-i2\pi 3 f a_1}\langle\vec{x} + \vec{a}_2| + |\vec{x} + \vec{\delta}\rangle\langle\vec{x} + \vec{a}_1| \\ &+ |\vec{x} + 2\vec{\delta}\rangle e^{-i2\pi 3 f(a_1 + \frac{1}{3})}\langle\vec{x} + \vec{a}_2| + |\vec{x} + 2\vec{\delta}\rangle\langle\vec{x} + \vec{a}_1| \\ &+ |\vec{x} + 2\vec{\delta}\rangle e^{-i2\pi 3 f(a_1 + \frac{2}{3})}\langle\vec{x} + \vec{a}_1 + \vec{a}_2| + \text{h.c.}]. \end{aligned} \tag{9}$$

The corresponding Harper equation is

$$\begin{aligned} &-(1 + e^{-i(k_y + 2\pi 3 f l)})\psi_l^b(\vec{k}) - e^{-ik_x}\psi_{l-1}^b(\vec{k}) - e^{-i(k_y + 2\pi 3 f(l + \frac{1}{3}))}\psi_l^c(\vec{k}) \\ &\quad -(e^{-ik_x} + e^{-i(k_x + k_y + 2\pi 3 f(l + \frac{2}{3}))})\psi_{l-1}^c(\vec{k}) = E(\vec{k})\psi_l^a(\vec{k}); \\ &-(1 + e^{-i(k_y + 2\pi 3 f l)})\psi_l^a(\vec{k}) - e^{ik_x}\psi_{l+1}^a(\vec{k}) = E(\vec{k})\psi_l^b(\vec{k}); \\ &-e^{i(k_y + 2\pi 3 f(l + \frac{1}{3}))}\psi_l^a(\vec{k}) - (e^{i(k_x + k_y + 2\pi 3 f(l + \frac{2}{3}))} + e^{ik_x})\psi_{l+1}^a(\vec{k}) = E(\vec{k})\psi_l^c(\vec{k}) \end{aligned} \tag{10}$$

where $l = 0, 1, \ldots, q - 1$ are the flavour indices and a, b, c are the three colour indices.

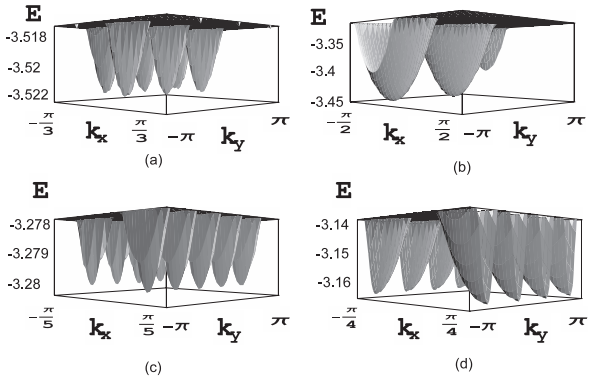

Figure 11. The lowest energy bands of a dice lattice at (a) $q = 9$, (b) $q = 6$, (c) $q = 5$, (d) $q = 4$.

For the simplest gauge shown in figure 10(b), we need to distinguish two general cases: $q = 3n$ and $q \neq 3n$. For $q \neq 3n$, we find out there are still two subcases: q is even and q is odd.

When q is small, we can solve the Harper equation analytically. For $q = 1$, which is the no magnetic field case, there are three bands: $\pm\sqrt{3 + 2(\cos k_x + \cos k_y + \cos(k_x - k_y))}$ and 0. The lowest band is $E(\vec{k}) = -\sqrt{3 + 2(\cos k_x + \cos k_y + \cos(k_x - k_y))}$. The minimum is at $(0, 0)$. For $q = 2$, all six bands are completely flat. The energies are $E = \sqrt{6}, 0, -\sqrt{6}$, each with degeneracy 2. For $q = 3$, there are also three bands: $\pm\sqrt{6 + 2A(k_x, k_y)}$ and 0. The lowest band is $E(\vec{k}) = -\sqrt{6 + 2A(k_x, k_y)}$, where $A(k_x, k_y) = \cos k_x + \cos k_y + \cos(k_x - k_y) + \cos(k_y + \frac{4\pi}{3}) + \cos(k_y - k_x + \frac{2\pi}{3}) + \cos(k_x + \frac{2\pi}{3})$. The two minima are at $(0, 0)$ and $(-\frac{2\pi}{3}, \frac{2\pi}{3})$.

In general, there are four cases in the dice lattice. (1) $q = 3n$, $\frac{-3\pi}{q} \leqslant k_x \leqslant \frac{3\pi}{q}$. There are q bands. We also need to distinguish two subcases. (1a) When n is odd, there are $2n$ minima at $(0, \frac{2\pi}{n}l)$ and $(-\frac{2\pi}{3n}, \frac{2\pi}{3n} + \frac{2\pi}{n}l), l = 0, \ldots, n - 1$. The $q = 9$ case is shown in figure 11(a). (1b) When n is even, there are n minima at $(-\frac{\pi}{3n}, \frac{2\pi}{3n} + \frac{2\pi}{n}l), l = 0, \ldots, n - 1$. The $q = 6$ case is shown in figure 11(b). For both cases, the bandwidth falls as $14.73\mathrm{e}^{-0.55q}$, as shown in figure 12(a). (2) $q \neq 3n$, $\frac{-\pi}{q} \leqslant k_x \leqslant \frac{\pi}{q}$. There are $3q$ bands. We also need to distinguish two subcases. 2(a) When q is odd, there are $2q$ minima at $(\frac{2\alpha\pi}{3q}, -\pi + \frac{\alpha\pi}{3q} + \frac{2\pi}{q}l)\alpha = \pm, l = 0, \ldots, q - 1$. The $q = 5$ case is shown in figure 11(c). The bandwidth falls as $0.54\mathrm{e}^{-0.54q}$, as shown in figure 12(b). (2b) When q is even, there are q minima at $(\frac{\pi}{q}, \frac{\pi}{q} + \frac{2\pi}{q}l), l = 0, \ldots, q - 1$. The $q = 4$ case is shown in figure 11(d); the bandwidth falls as $1.01\mathrm{e}^{-0.54q}$, as shown in figure 12(c).

It seems to us that all the four cases have the same c within numerical errors, but different magnitude A.

6. Kagome lattice

The Kagome lattice is not a Bravais lattice either; it can be thought of as an underlying parallelogram Bravais lattice with two primitive lattice vectors $\vec{a}_1 = \hat{x}, \vec{a}_2 = \frac{1}{2}\hat{x} + \frac{\sqrt{3}}{2}\hat{y}$ plus a three-point basis labelled a, b, c located at $\vec{x}, \vec{x} + \vec{a}_1/2, \vec{x} + \vec{a}_2/2$, as shown in figure 13. Note that the Kagome lattice contains both triangles and hexagons.

We are looking at the Hofstadter band of vortices hopping around a Kagome lattice in the presence of magnetic flux $f = p/q$ per triangle and $6f$ flux quantum per hexagon. So overall, there are $8f$ flux quanta per parallelogram. For the simplest gauge chosen in figure 13(b), the

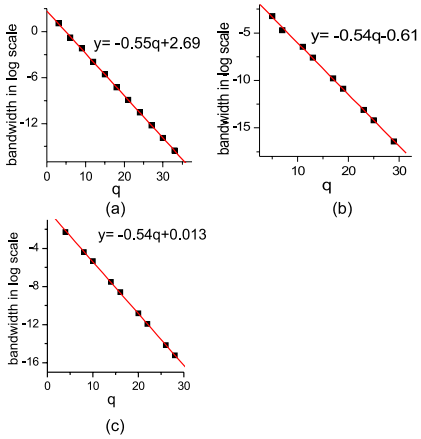

Figure 12. The bandwidths of a dice lattice versus q: (a) $q = 3n$, (b) $q \neq 3n$ and odd, (c) $q \neq 3n$ and even.

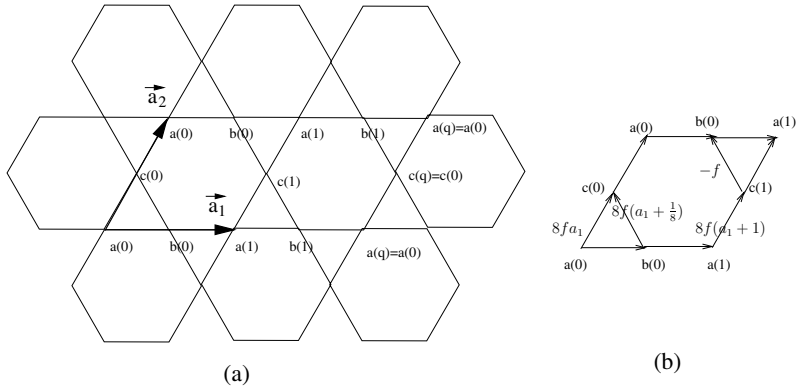

Figure 13. Kagome lattice: (a) magnetic unit cell of a Kagome lattice, (b) phase factors on bonds; 0 phase factors are not shown.

Hamiltonian is

$$H = -t\sum_{\vec{x}}\Bigg[\left|\vec{x}+\frac{\vec{a}_1}{2}\right\rangle\langle\vec{x}| + \left|\vec{x}+\frac{\vec{a}_2}{2}\right\rangle e^{i2\pi 8fa_1}\langle\vec{x}| + |\vec{x}+\vec{a}_1\rangle\left\langle\vec{x}+\frac{\vec{a}_1}{2}\right| + |\vec{x}+\vec{a}_2\rangle\left\langle\vec{x}+\frac{\vec{a}_2}{2}\right| + \left|\vec{x}+\frac{\vec{a}_1}{2}+\vec{a}_2\right\rangle e^{-i2\pi f}\left\langle\vec{x}+\vec{a}_1+\frac{\vec{a}_2}{2}\right| + \left|\vec{x}+\frac{\vec{a}_2}{2}\right\rangle e^{i2\pi 8f(a_1+\frac{1}{8})}\left\langle\vec{x}+\frac{\vec{a}_1}{2}\right| + \text{h.c.}\Bigg]. \tag{11}$$

The corresponding Harper equation is

$$\begin{aligned}
&-\psi_l^b(\vec{k}) - e^{ik_x}\psi_{l-1}^b(\vec{k}) - (e^{ik_y}+e^{-i2\pi 8fl})\psi_l^c(\vec{k}) = E(\vec{k})\psi_l^a(\vec{k});\\
&-\psi_l^a(\vec{k}) - e^{-ik_x}\psi_{l+1}^a(\vec{k}) - e^{-i2\pi 8f(l+\frac{1}{8})}\psi_l^c(\vec{k}) - e^{-i(2\pi f+k_x-k_y)}\psi_{l+1}^c(\vec{k}) = E(\vec{k})\psi_l^b(\vec{k});\\
&-(e^{-ik_y}+e^{i2\pi 8fl})\psi_l^a(\vec{k}) - e^{i2\pi 8f(l+\frac{1}{8})}\psi_l^b(\vec{k})\\
&\quad -e^{i(2\pi f+k_x-k_y)}\psi_{l-1}^b(\vec{k}) = E(\vec{k})\psi_l^c(\vec{k}).
\end{aligned} \tag{12}$$

For the gauge chosen in figure 13(a), we can solve the spectra at $q = 1, 2, 4, 8$ exactly, because for all the four cases, we only need to solve a 3 by 3 matrix whose

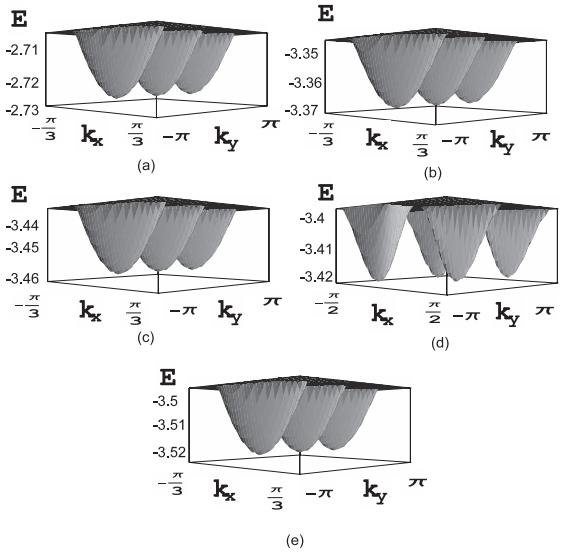

Figure 14. The lowest energy bands of a Kagome lattice at (a) $q = 3$, (b) $q = 6$, (c) $q = 12$, (d) $q = 16$, (e) $q = 24$.

secular equation is a cubic equation $\lambda^3 - (4 + A(k_x, k_y))\lambda + 2\cos(\frac{2\pi}{q})A(k_x, k_y) = 0$ where $A(k_x, k_y) = 2 + 2(\cos k_x + \cos k_y + \cos(k_x - k_y))$. There are three bands. For $q = 1$ which is the no magnetic field case, the three bands are $-1 \pm \sqrt{1 + A(k_x, k_y)}, 0$. The lowest band is $E(\vec{k}) = -1 - \sqrt{1 + A(k_x, k_y)}$ whose minimum is at $(0, 0)$. For $q = 2$, the three bands are $-2, 1 - \sqrt{1 + A(k_x, k_y)}, 1 + \sqrt{1 + A(k_x, k_y)}$. We can see that the lowest band is completely flat; the second band touches the lowest band at $\vec{k} = (0, 0)$ where the gap vanishes! For $q = 4$, the three bands are $\pm\sqrt{4 + A(k_x, k_y)}, 0$. The lowest band is $E(\vec{k}) = -\sqrt{4 + A(k_x, k_y)}$. The minimum is at $(0, 0)$. For $q = 8$, we need to solve the cubic equation numerically; the minimum of the lowest band is found to be at $(0, 0)$.

In general, there are five cases in a Kagome lattice. (1) $q = n$ is odd, $\frac{-\pi}{q} \leqslant k_x \leqslant \frac{\pi}{q}$. There are q minima in the spectrum at $(0, \frac{2\pi}{q}l), l = 0, 1, \ldots, q - 1$. The $q = 3$ case is shown in figure 14(a). We find that the bandwidth does not satisfy the exponential law as shown in figure 15(a). (2) $q = 2n$ with n odd, $\frac{-2\pi}{q} \leqslant k_x \leqslant \frac{2\pi}{q}$. There are $\frac{q}{2}$ minima at $(0, \frac{4\pi}{q}l), l = 0, 1, \ldots, q/2 - 1$. The $q = 6$ case is shown in figure 14(b). But when $q = 2$, as shown above, the lowest energy band is completely flat. From figure 15(b), we can clearly see two separate straight lines. We divide the data into separate sets. For set 1 in figure 15(b.1), the bandwidth falls as $0.33e^{-0.20q}$. For set 2 in figure 15(b.2), the bandwidth falls as $0.10e^{-0.20q}$. (3) $q = 4n$ with n odd, $\frac{-4\pi}{q} \leqslant k_x \leqslant \frac{4\pi}{q}$. There are $\frac{q}{4}$ minima at $(0, \frac{8\pi}{q}l), l = 0, \ldots, q/4 - 1$. The $q = 12$ case is shown in figure 14(c). The bandwidth falls as $2.46e^{-0.21q}$ as shown in figure 15(c). (4) $q = 8n$, $\frac{-8\pi}{q} \leqslant k_x \leqslant \frac{8\pi}{q}, l = 0, 1, \ldots, q/8 - 1$. There are also two subcases. (4a) When n is even, there are $2n$ minima at $(-\frac{\alpha\pi}{3n}, -\alpha\pi + \frac{\alpha\pi}{3n} + \frac{2\pi}{n}l)\alpha = \pm$. The $q = 16$ case is shown in figure 14(e). (4b) When n is odd, there are n minima at $(0, \frac{16\pi}{q}l)$. The $q = 24$ case is shown in figure 14(d). For both cases, the bandwidth falls as $13.87e^{-0.21q}$, as shown in figure 15(d). There are $3n$ bands in all these cases.

It seems to us that all the five cases have the same c within numerical errors, but different magnitude A.

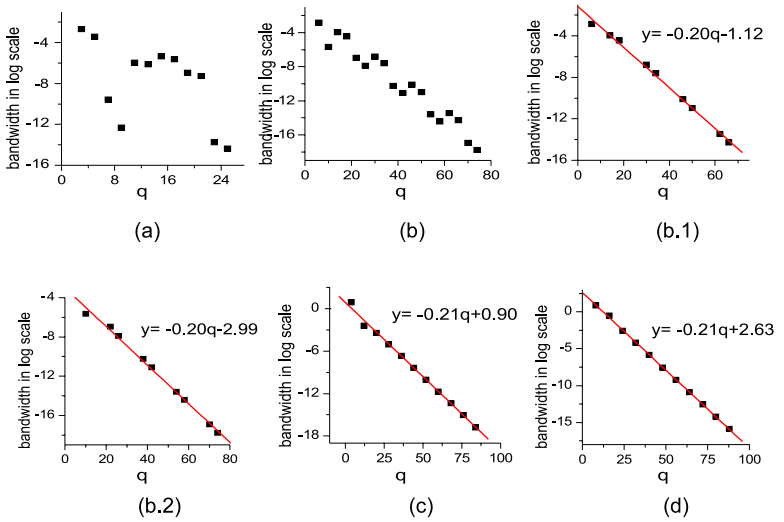

Figure 15. The bandwidth of the bands in a Kagome lattice: (a) q is odd, (b) $q = 2n$ with n odd, (b.1) $q = 2n$ case 1, (b.2) $q = 2n$ case 2, (c) $q = 4n$ with n odd, (d) $q = 8n$.

7. Summary and conclusions

In this paper, we have studied the energy spectra of the Hofstadter band of vortices hopping on five lattices in the presence of magnetic flux $f = p/q$ per smallest plaquette. Our results on dice and Kagome lattices are new and interesting. The number of the energy bands and the number of minima in the lowest band in the five lattice are listed in table 1.

Table 1. The number of minima of the lowest Hofstadter bands in the five lattices. N_q^n means $q = n$. Suffices e and o mean even and odd. We also list the total number of bands just below each case. At $q = 2$, the lowest band in Kagome and dice lattices is completely flat.

	Square	Honeycomb	
Bipartite	$N_q^n = q$	$N_q^n = \begin{cases} 2n, & n = \mathrm{e} \\ n, & n = \mathrm{o} \end{cases}$	
	q bands	$2q$ bands	
	Triangular	Dice	Kagome
Frustrated	$N_q^{2n} = \begin{cases} n, & n = \mathrm{e} \\ 2n, & n = \mathrm{o} \end{cases}$, $\frac{q}{2}$ bands	$N_q^{3n} = \begin{cases} n, & n = \mathrm{e} \\ 2n, & n = \mathrm{o} \end{cases}$, $3n$ bands	$N_q^n = n = \mathrm{o}$, $N_q^{2n} = n = \mathrm{o}$
	$N_q^{\mathrm{o}} = q$, q bands	$N_{q\neq 3n}^{\mathrm{e}} = q$, $N_{q\neq 3n}^{\mathrm{o}} = 2q$	$N_q^{4n} = n = \mathrm{o}$, $N_q^{8n} = \begin{cases} 2n, & n = \mathrm{e} \\ n, & n = \mathrm{o} \end{cases}$
		Above two have $3q$ bands	All cases have $3n$ bands

It was argued in [9] that for large q, the bandwidth of the lowest energy Hofstadter band in a square lattice scales as $W = A\mathrm{e}^{-cq}$ with $c \sim 1$. We believe that although the argument seems reasonable, it is far from being convincing. So it is important to test this argument by quantitative numerical calculations. We tested the rule by numerically calculating the

bandwidths of the lowest Hofstadter bands in the five lattices. We found that this rule is indeed satisfied for all the lattices even for smallest values of $q = 1$ apart from the Kagome lattice for q odd. For Kagome and dice lattices, the lowest band is completely flat at $q = 2$. The results of (A, c) for the five lattices are listed in the table 2.

Table 2. The bandwidth parameters (A, c) of the lowest Hofstadter bands in the five lattices. Suffix e (o) means q is even (odd). At $q = 2$, the lowest band in the Kagome and dice lattices is completely flat.

Square	Honeycomb	Triangle	Dice	Kagome
$(26.05, 1.20)$	$(11.82, 1.66)$	$(55.70, 0.83)_{\mathrm{e}}$	$(14.73, 0.55)_{3n}$	Odd, not apply
		$(9.21, 0.82)_{\mathrm{o}}$	$(1.01, 0.54)_{\mathrm{e}\neq 3n}$	$(0.33, 0.20)_{2n,1}$
				$(0.10, 0.20)_{2n,2}$
			$(0.54, 0.54)_{\mathrm{o}\neq 3n}$	$(2.46, 0.21)_{4n}$
				$(13.87, 0.21)_{8n}$

From table 2, it is easy to see that for a given lattice, although the prefactor A could be different for different cases, the value of c remains the same within numerical error for a given lattice. For a Kagome lattice when q is odd, the bandwidth does not satisfy any exponential decay law. However, in all other cases, the bandwidths satisfy the exponential laws. The peculiarity of the Kagome lattice may be related to the fact that, in contrast to all the other four lattices, a Kagome lattice has both triangles which enclose f flux quanta and hexagons which enclose 6f flux quantum.

As was said in the introduction, the first motivation to study the bandwidth is to look at the valid regime of dual vortex approach in the five lattices. If q is too large, the bandwidth becomes too small, and the dual vortex approach may not be valid anymore. For example, on a square lattice, when $q = 4$, $W = 0.21$ is already very small. This fact puts some doubts on the results of CDW formations in high temperature superconductors in [9], where q values as large as 8, 16, 32 are used. In fact, large q means *very dilute* boson density in the direct lattice. In this case, the superfluid is probably the only ground state anyway, except there are extremely exotic long range interactions in equation (1) which may stabilize the CDW and VBS. Fortunately, $q = 2$ (which is the smallest non-trivial case) in a honeycomb lattice was applied by one of the authors to study helium and hydrogen adsorption problems on various substrates in [12].

The second motivation is to study the tendency for interacting bosons to form a superfluid in the five lattices. The bandwidth is proportional to the vortex hopping matrix element, so the smallness of bandwidth favours the localization of the vortices, and therefore enhances the tendency to form a superfluid. At given q, the bandwidth W decreases in the order of triangle, square and honeycomb lattice. The corresponding direct lattices are honeycomb, square and triangular lattices whose coordination numbers are 3, 4 and 6. It is known that the higher the coordination, the easier it is for bosons to get into the ordered superfluid state. The conclusions achieved in the dual lattice are indeed consistent with our intuition in the direct lattice.

As shown in the table 1, when $q = 2$, the lowest bands in both dice and Kagome lattices are flat. In a dice lattice, the gap between the second flat band and the lowest flat band is $\sqrt{6}$. However, in a Kagome lattice, the gap between the second dispersive band and the lowest flat band vanishes at $\vec{k} = (0, 0)$, so the second dispersive band cannot be ignored even in the lowest energy limit. In a dice lattice, all the three bands are flat, the vortices are completely inert, and the interactions certainly favour the localization of the vortices. This indicates that for the original boson at half filling ($q = 2$) with nearest neighbour hopping on the Kagome lattice, there could only be a superfluid state. Slightly away from half filling, it was known that the superfluid state is stable against a small number of vacancies or interstitials; we expect the

superfluid state to remain stable. This is in sharp contrast to bosons at half filling hopping on a triangular lattice where there is a dispersion in the lowest band as shown in this paper. Due to the competition between the kinetic energy and the interactions between the vortices, there is a transition from a superfluid to a supersolid state as shown in [7]. The $q = 2$ cases for square [9] and honeycomb [12] lattices were shown to have a CDW or VBS to superfluid transition in the Ising or easy-plane limit. Slightly away from half filling, in the CDW or VBS side, it was shown in [12] that there must be a CDW or VBS supersolid state intervening between the commensurate CDW or VBS to incommensurate CDW or VBS in the Ising or easy-plane limit. Obviously, the behaviours of bosons on a Kagome lattice at or near half filling ($q = 2$) are quite distinct from those in square, honeycomb and triangular lattices.

It is important to stress that the exactly flat bands at $q = 2$ for the dice lattice are completely due to the special lattice structure of the dice lattice which localizes the vortices. The dual vortex theory immediately leads to the boson superfluid state in the Kagome lattice. Of course, the bandwidth goes to zero at large q in any lattice. However, as stated previously, the dual vortex theory is no longer valid at sufficiently large q.

The main body of this paper only discusses the $p = 1$ case. Taking the complex conjugate of the Harper equation $H\psi(\vec{k}) = E(\vec{k})\psi(\vec{k})$ leads to $H^*\psi^*(\vec{k}) = E(\vec{k})\psi^*(\vec{k})$. Obviously, H^* corresponds to $-f$, which is equivalent to $1-f = 1-p/q$, so $p = 1$ has the same energy spectra as $p = q - 1$ for non-interacting vortices. Of course, vortex interactions will not have the periodicity $f \to 1+f$ anymore, so $p = 1$ and $p = q-1$ in equation (1) may not be equivalent.

In a future publication, we will try to answer the following by analytical methods similar to the ones used in [19]. (1) Why is $W = Ae^{-cq}$ satisfied at even the smallest value of q? Is this a unique feature of any tight binding model? (2) For different cases on triangular and dice lattices and the Kagome lattice for q even listed in table 2, why is c the same within numerical error, while A differs? (3) What is the bandwidth rule in a Kagome lattice for odd q? We will also construct MSGs for the dice and Kagome lattices to understand the energy spectra structure in table 1.

Acknowledgment

J Ye thanks E Fradkin for helpful discussions.

Appendix

In this appendix, we simply list the Harper equations in the symmetric method first used in [9]. They may look different from those corresponding equations obtained by the MBZ method used in the main text, but we show that both lead to the same Hofstadter bands in the five lattices. This check ensures the correctness of the results in the main text.

(1) Square lattice

$$-e^{-ik_y}\psi_{l-1} - 2\cos(k_x + 2\pi f l)\psi_l - e^{ik_y}\psi_{l+1} = E\psi_l \tag{A.1}$$

where $l = 0, \ldots, q-1$; $\frac{-\pi}{q} \leqslant k_x \leqslant \frac{\pi}{q}$

(2) Honeycomb lattice

$$\begin{aligned} -(1 + e^{i(k_x+2\pi f l)})\psi_l^a - e^{ik_y}\psi_{l+1}^a &= E\psi_l^b \\ -(1 + e^{-i(k_x+2\pi f l)})\psi_l^b - e^{-ik_y}\psi_{l-1}^b &= E\psi_l^a \end{aligned} \tag{A.2}$$

where $l = 0, \ldots, q-1$; $-\frac{\pi}{q} \leqslant k_x \leqslant \frac{\pi}{q}$.

(3) Triangular lattice

$$-(e^{-ik_y}+e^{-i(k_x+k_y+2\pi f(2l-1))})\psi_{l-1}-(e^{ik_2}+e^{i(k_x+k_y+2\pi f(2l+1))})\psi_{l+1} \\ -2\cos(k_x+2\pi fl)\psi_l = E\psi_l \tag{A.3}$$

where $l=0,\ldots,q-1$, $\frac{-\pi}{q}\leqslant k_x\leqslant\frac{\pi}{q}$ for q odd, $l=0,\ldots,q/2-1$, $\frac{-2\pi}{q}\leqslant k_x\leqslant\frac{2\pi}{q}$ for q even.

(4) Dice lattice

$$\begin{aligned}
&-(1+e^{i(k_x+2\pi 3fl)})\psi_l^a-e^{ik_2}\psi_{l+1}^a=E\psi_l^b;\\
&-e^{i(k_x+2\pi 3fl)}\psi_l^a-(e^{i(k_y-2\pi f)}+e^{i(k_x+k_y+2\pi 3f(l+1)-4\pi f)})\psi_{l+1}^a=E\psi_l^c;\\
&-(1+e^{-i(k_x+2\pi 3fl)})\psi_l^b-e^{-ik_y}\psi_{l-1}^b-e^{-i(k_x+2\pi 3fl)}\psi_l^c\\
&\quad-(e^{-i(k_y-2\pi f)}-e^{-i(k_x+k_y+2\pi 3fl-4\pi f)})\psi_{l-1}^c=E\psi_l^a
\end{aligned} \tag{A.4}$$

where for $q\neq 3n$, $l=0,\ldots,q-1$, $\frac{-\pi}{q}\leqslant k_x\leqslant\frac{\pi}{q}$. For $q=3n$, $l=0,\ldots,q/3-1$, $\frac{-3\pi}{q}\leqslant k_x\leqslant\frac{3\pi}{q}$.

(5) Kagome lattice

$$\begin{aligned}
&-(1+e^{i(k_x+2\pi 8fl)})\psi_l^a-e^{-i2\pi f}\psi_{l+1}^c-e^{-i(2\pi f+k_y-k_x-2\pi 8fl)}\psi_l^c=E\psi_l^b;\\
&-\psi_{l-1}^a-e^{i2\pi f}\psi_{l-1}^b-e^{ik_y}\psi_l^a-e^{i(2\pi f+k_y-kx-2\pi 8fl)}\psi_l^b=E\psi_l^c;\\
&-(1+e^{-i(k_x+2\pi 8fl)})\psi_l^b-\psi_{l+1}^c-e^{-ik_y}\psi_l^c=E\psi_l^a
\end{aligned} \tag{A.5}$$

where for q odd, $l=0,\ldots,q-1$, $\frac{-\pi}{q}\leqslant k_x\leqslant\frac{\pi}{q}$, for $q=2n$ with n odd, $l=0,\ldots,q/2-1$, $\frac{-2\pi}{q}\leqslant k_x\leqslant\frac{2\pi}{q}$. For $4n$ with n odd, $l=0,\ldots,q/4-1$, $\frac{-4\pi}{q}\leqslant k_x\leqslant\frac{4\pi}{q}$. For $q=8n$, $l=0,\ldots,q/8-1$, $\frac{-8\pi}{q}\leqslant k_x\leqslant\frac{8\pi}{q}$.

References

[1] Bretz M, Dash J G, Hickernell D C, McLean E O and Vilches O E 1973 *Phys. Rev.* A **8** 1589–615
[2] Bruch L W, Cole M W and Zaremba E 1997 *Physics Absorption: Force and Phenomena* (Oxford: Clarendon)
[3] O'Hara K M, Hemmer S L, Gehm M E, Granade S R and Thomas J E 2002 *Science* **298** 2179
[4] Greiner M, Mandel O, Esslinger T and Bloch I 2002 *Nature* **415** 39–44
[5] Fisher M P A, Weichman P B, Grinstein G and Fisher D S 1989 *Phys. Rev.* B **40** 546
[6] Batrounil G C *et al* 1995 *Phys. Rev. Lett.* **74** 2527
[7] Murthy G, Arovas D and Auerbach A 1997 *Phys. Rev.* B **55** 3104–21
[8] Ye J 1998 *Phys. Rev.* B **58** 9450–9
[9] Balents L, Bartosch L, Burkov A, Sachdev S and Sengupta K 2005 *Phys. Rev.* B **71** 144508
[10] Hofstadter D R 1976 *Phys. Rev.* B **14** 2239–49
Zak J 1964 *Phys. Rev.* **134** A1602–6
Zak J 1964 *Phys. Rev.* **134** A1607–11
[11] Burkov A A and Balents L 2005 *Phys. Rev.* B **72** 134502
[12] Ye J 2005 *Preprint* cond-mat/0503113
[13] Dasgupta C and Halperin B I 1981 *Phys. Rev. Lett.* **47** 1556–60
[14] Wiechert H, Kortmann K-D and Stüßer N 2004 *Phys. Rev.* B **70** 125410
[15] Crowell P A and Reppy J D 1993 *Phys. Rev. Lett.* **70** 3291–4
[16] Crowell P A and Reppy J D 1996 *Phys. Rev.* B **53** 2701–18
[17] Ye J, unpublished
[18] After the paper was finished, we realized that Yi X *et al* discussed Kagome grid superconducting wire network in Yi X *et al* 2003 *Phys. Rev.* B **67** 104505 (The focus in our paper is completely different)
[19] Thouless D J, Kohmoto M, Nightingale M P and den Nijs M 1982 *Phys. Rev. Lett.* **49** 405–8
[20] After this paper was submitted, we learned a related and independent work by Sengupta K, Isakov S V and Kim Y B 2006 *Preprint* cond-mat/0601175